encit 2020

ABCM Associação Brasileira de Engenharia e Ciências Mecânicas

18th Brazilian Congress of Thermal Sciences and Engineering
November 16–20, 2020 (Online)

ENC-2020-0381
THE CHOICE OF THE CONSTITUTIVE EQUATION AND ITS EFFECT ON THE PLANAR CHANNEL FLOW SOLUTION

Luiz Paulo Borges Miranda
Daniel Dall'Onder dos Santos
Federal University of Uberlândia, Av. João Naves de Ávila 2121, Uberlândia, MG, 38408-100, Brazil
luiz.miranda@ufu.br
dallonder@ufu.br

Flavia Schwarz Franceschini Zinani
UNISINOS, Av. Unisinos 950, São Leopoldo, RS, 93.022-750, Brazil
fzinani@unisinos.br

Abstract. *In the present work, fourteen constitutive functions were used to evaluate their effects over the flow parameters of a fully developed flow in a planar channel with an imposed pressure gradient. A virtual set of rheological data was created using the modified SMD constitutive function. Then, this virtual set was used at curve fitting process with fourteen constitutive functions. The parameters of the fitted curves were used to semi-analytically solve the fully developed flow in a planar channel with an imposed pressure gradient. The pressure gradients were chosen to kept the Reynolds number of the flow under the range of $Re \leq 100$, assuring the laminar regime. The r^2 of the fitting process and the flow rate (Q) were compared, searching for a convergence between the models. There is only convergence of results in some particular cases, and usually the difference of flow rate between models is higher than 10%. For this range of Reynolds number, some constitutive functions can not achieve the high shear rate plateau, decreasing the influence of these parameters and allowing models with less parameters to have an equivalent or even better better fit.*

Keywords: *semi analytic solution, viscoplastic behavior, planar channel, fully developed flow*

1. INTRODUCTION

In the beginning of the 18th century, Isaac Newton proposed a linear constitutive function to correlate the shear stress and the shear rate, known today as the Newtonian viscosity model. Although this model can fit well several applications, especially those involving water and air, some fluids can show a more complex behavior, and in the beginning of the 20th century Bingham (1917) proposed a new constitutive function where the shear stress domain is divided into two different conditions: if the shear stress is under a certain amount of stress, the viscosity is considered infinity; if the shear stress is above this quantity, it behaves like a Newtonian fluid. A fluid that presents infinite viscosity, or in other words, is solid under a certain level of stress, is the classical definition of a viscoplastic fluid. With the development of more precise rheometers, nowadays the infinite viscosity is seen as a very high viscosity plateau that happens at levels of stress under the yield stress threshold.

As there were still some rheological behavior that neither Newtonian nor the Bingham model could predict, later in the 1920s power-law functions were proposed to model the viscosity behavior, the power-law model and the Herschel-Bulkley model, the later being able to predict the viscoplastic behavior (Bird *et al.*, 1987).

Although the constitutive functions cited above have their own characteristics and applications, the choice of which to adopt is not trivial. First, a real fluid behavior can be much more complex than these functions can predict. Second, depending on the range of the shear rate involved in the application, a more complex fluid can be modeled by a simpler function. And finally, choosing a complex function to model a fluid can be computationally demanding. The Newtonian, Bingham, Herschel-Bulkley, and power-law models are the base for several others that try to model more complex behaviors and applications.

Casson (1959) proposed a two parameter model as an alternative to the Bingham model, showing that different artifices can be used to model the same behavior without increasing the number of parameters. Cross (1965) and Carreau (2006) have both proposed four-parameter models, that can be seen as extensions of the power-law model, because they predict viscosity plateaus for low and high shear rates and have a power-law region. This way, these functions can fit a larger range of the shear rate. The Carreau model is also known as Bird-Carreau model, and is a particular case of the Carreau-Yasuda model, which has one parameter more. The Casson and Carreau modelas are mainly used in the food industry and also to model the blood rheological behavior.

With the development of the computational fluid mechanics, it was demanded the models to have a new set of characteristics to ease their application. The Bingham model has three main regularizations, proposed by Bercovier and Engelman (1980), O'Donovan and Tanner (1984), and Papanastasiou (1987), the later being the most known and employed. These functions have three parameters and are continuous, but the derivatives of the bi-viscosity model (O'Donovan and Tanner, 1984) are not continuous. Another characteristic of the bi-viscosity model is that the viscosity does not tend to infinity when the shear rate tends to zero, as the Papanastasiou model does. The Papanastasiou model is an exponential function, whilst Bercovier and Engelman model, or simply BE model, is a rational function, but both have a regularization parameter.

The Herschel-Bukley model also have its regularizations, being the most used an adaptation of the Papanastasiou regularized Bingham model – referred henceforth in this work only as regularized Herschel-Bulkley model, or simply rHB. Other regularization examples are the model proposed by de Souza Mendes and Dutra (2004) and its variations (de Souza Mendes, 2007) (Santos *et al.*, 2011). The regularized Herschel-Bulkley and the SMD models have four parameters, are continuous with continuous derivatives and are exponential functions. The regularized Herschel-Bulkley model still has a numerical regularization parameter and the viscosity tends to the infinity when the shear rate tends to zero. The SMD model does not have a regularization parameter, as all its parameters are purely rheological. The harmonic viscoplastic model (Ferreira, 2018), or HVP model, and a adaptation of the SMD function to model a high shear rate plateau (de Souza Mendes, 2007) can also be seen as alternatives to the Herschel-Bukley model. These last two functions have five parameters and they are able to fit a larger range of shear rate. Furthermore, de Souza Mendes and Dutra (2004) demonstrated that these models are able to fit flow curves of a large number of different products.

In this work, a SMD function were used to create a virtual set of rheological data regarding to hypothetical fluid with viscoplastic behavior. Then, a curve fitting process was performed with this set of data with fourteen other constitutive functions. The parameters of the fitted curves were used to semi-analytically solve the fully developed flow in a planar channel with an imposed pressure gradient. The r^2 of the fitting process and the flow rate (Q) were compared, searching for a convergence between the models. Although hypothetical, the fluid is based on real data obtained in rheological measurements for Carbopol 0.12% wt aqueous solution presented by de Souza Mendes and Dutra (2004).

2. METHODOLOGY

2.1 Mechanical model and geometry

The mathematical model for the steady state flow of a generalized Newtonian fluid through a two-dimensional planar channel consists of the balance equations of mass, and momentum for a control volume:

$$\begin{aligned} &\nabla \cdot \mathbf{u} = 0 \\ &\rho(\nabla \mathbf{u})\mathbf{u} = -\nabla p + \nabla \cdot \boldsymbol{\tau} \end{aligned} \tag{1}$$

where **u** is the velocity vector, ρ is the density, p is the hydrostatic pressure, and $\boldsymbol{\tau}$ is the extra-stress tensor defined by the following constitutive equation:

$$\boldsymbol{\tau} = 2\eta(\dot{\gamma})\mathbf{D}(\mathbf{u}) \tag{2}$$

where **D**(**u**) and $\dot{\gamma}$ are defined as:

$$\mathbf{D}(\mathbf{u}) = \frac{1}{2}(\nabla \mathbf{u} + \nabla \mathbf{u}^T) \tag{3}$$

$$\dot{\gamma} = \sqrt{2tr\mathbf{D}(\mathbf{u})^2} \tag{4}$$

Adopting the condition of fully developed flow and integrating for y, Eq. (1-4) becomes:

$$\begin{aligned} &y\frac{dp}{dx} = \tau \\ &\tau = \eta(\dot{\gamma})\dot{\gamma} \\ &\dot{\gamma} = \frac{du}{dy} \end{aligned} \tag{5}$$

where y is the vertical position of the analyzed point, where zero is the symmetry line and one is the upper channel wall, and u is the velocity in the x direction. The schematic representation of the geometry is shown in Fig. 1. The extra-stress tensor has only one non null value, and is represented by τ.

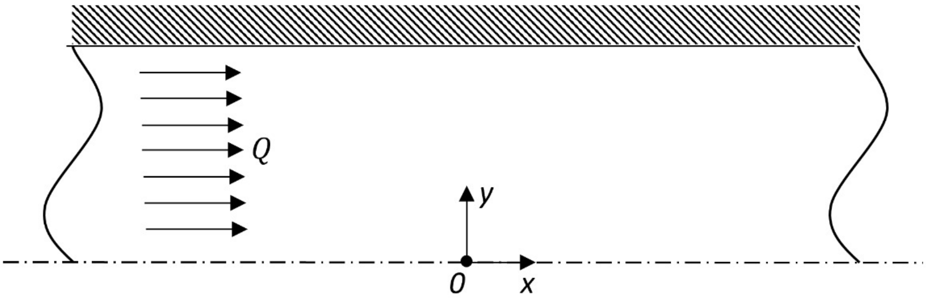

Figure 1. Schematic representation of the adopted geometry.

Fourteen functions were used in this study to model the non-Newtonian viscosity. Not all of then can model the viscoplastic behavior, but they are considered here to highlight the importance of modeling accordingly this effect. The fourteen functions are shown in Tab. 1.

Table 1: Vicosity functions employed in this work.

Model	Equation
Newtonian	$\tau = \mu\dot{\gamma}$ (6)
Power-law	$\tau = K\dot{\gamma}^n$ (7)
Power-law (with boundaries)	$\tau = \eta_0\dot{\gamma} \quad for \ \dot{\gamma} < \dot{\gamma}_0$ $\tau = K\dot{\gamma}^n \quad for \ \dot{\gamma}_0 < \dot{\gamma} < \dot{\gamma}_2$ $\tau = \eta_\infty\dot{\gamma} \quad for \ \dot{\gamma} > \dot{\gamma}_2$ (8)
Bingham	$\tau = \tau_0 + \mu_p\dot{\gamma} \quad for \ \tau \geq \tau_0$ $\dot{\gamma} = 0 \quad for \ \tau < \tau_0$ (9)
Bingham (Papanastasiou regularization)	$\tau = (1 - e^{-m\dot{\gamma}})\tau_0 + \mu_p\dot{\gamma}$ (10)
Bingham (Bercovier and Engelman regularization)	$\tau = \dfrac{\tau_0\dot{\gamma}}{\delta + \dot{\gamma}} + \mu_p\dot{\gamma}$ (11)
Casson	$\tau = \left(\sqrt{\tau_0} + \sqrt{K\dot{\gamma}}\right)^2$ (12)
Herschel-Bulkley	$\tau = \tau_0 + K\dot{\gamma}^n \quad for \ \tau \geq \tau_0$ $\dot{\gamma} = 0 \quad for \ \tau < \tau_0$ (13)
Regularized Herschel-Bulkley (rHB)	$\tau = [1 - exp\,(-m\dot{\gamma})])\tau_0 + K\dot{\gamma}^n$ (14)

Continue on the next page

Table 1: Vicosity functions employed in this work (cont.).

Model	Equation
Carreau	$\tau = \left\{ \eta_\infty + \eta_0 \left[1 + (K\dot{\gamma})^2 \right]^{\frac{n-1}{2}} \right\} \dot{\gamma} \quad (15)$
Cross	$\tau = \left(\eta_\infty + \frac{\eta_0 - \eta_\infty}{1 + K\dot{\gamma}^n} \right) \dot{\gamma} \quad (16)$
Bi-Viscosity	$\tau = \eta_0 \dot{\gamma} \quad for\ \dot{\gamma} < \frac{\tau_0}{\eta_0}$; $\tau = \tau_0 + \eta_\infty \left(\dot{\gamma} + \frac{\tau_0}{\eta_0} \right) \quad for\ \dot{\gamma} \geq \frac{\tau_0}{\eta_0} \quad (17)$
Harmonic viscoplastic	$\tau = \dot{\gamma} \left(\frac{1}{\eta_0} + \frac{\dot{\gamma}}{\tau_0 + K\dot{\gamma}^n + \eta_\infty \dot{\gamma}} \right) \quad (18)$
SMD (de Souza Mendes and Dutra, 2004)	$\tau = \left[1 - exp \left(\frac{-\eta_0}{\tau_0} \dot{\gamma} \right) \right] (\tau_0 + K\dot{\gamma}^n) \quad (19)$
SMD_∞ (de Souza Mendes, 2007)	$\tau = \left[1 - exp \left(\frac{-\eta_0}{\tau_0} \dot{\gamma} \right) \right] (\tau_0 + K\dot{\gamma}^n) + + \eta_\infty \dot{\gamma} \left[1 - exp \left(\frac{\eta_\infty}{K\dot{\gamma}^{n-1}} \right) \right] \quad (20)$

In Table 1, μ is the newtonian viscosity; μ_p is the plastic viscosity, as referred to in the Bingham literature; K is the consistency index; n is the power-law index; η_0 and η_∞ are, respectively, the apparent viscosity for very low and high values of the shear rate and τ_0 is the yield stress limit of the material. The parameters δ and m are regularization parameters, and in this work they are also defined by the curve fitting process, as they can significantly change the fluid behavior. Benmoussa *et al.* (2017) and Burgos *et al.* (1999) have already studied the effect of these parameters over the fluid behavior.

Figure 2 shows the apparent viscosity as a function of the shear rate for different values of n, adopting the SMD_∞ model. It is possible to identify four main regions:

- The high apparent viscosity plateau for low shear rates: it is the characteristic region of viscoplastic fluids. The shear rate is lower than $\dot{\gamma}_0$, defined as:

$$\dot{\gamma}_0 = \frac{\tau_0}{\eta_0} \tag{21}$$

- The transition region: the transition between the high apparent viscosity plateau and the power law region, characterized by an abrupt decrease of the apparent viscosity. The shear rate is higher than $\dot{\gamma}_0$, but lower than $\dot{\gamma}_1$, with the later defined as:

$$\dot{\gamma}_1 = \left(\frac{\tau_0}{K} \right)^{\frac{1}{n}} \tag{22}$$

- The power law region: the region where the apparent viscosity behavior approaches the power-law model. The shear rate is higher than $\dot{\gamma}_1$, but lower than $\dot{\gamma}_2$, with the later expressed by:

$$\dot{\gamma}_2 = \left(\frac{K}{\eta_\infty} \right)^{1/(1-n)} \tag{23}$$

- The high shear rates viscosity plateau: as seen in Fig. 2, Eq. 20 models a high shear rate viscosity plateau when $n < 1$ to prevent the apparent viscosity from tending to a zero value.

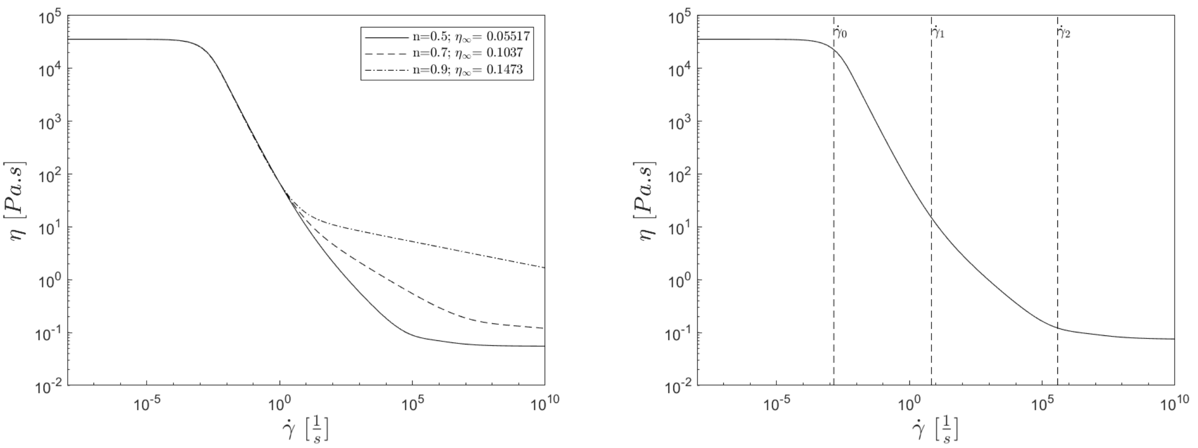

(a) (b)

Figure 2. η as function of $\dot\gamma$, adopting the SMD$_\infty$ model (Eq. 20): (a) for different values of n with $\eta_0 = 35600\ Pa.s$, $K = 16.65\ Pa.s^n$, and $\tau_0 = 50.25\ Pa$; (b) a graphical representation of $\dot\gamma_0$, $\dot\gamma_1$, and $\dot\gamma_2$ for $n = 0.5$.

2.2 Dimensionless groups of interest

In this work, the flow curve of the fluid was defined *a priori*, so the influence of the chosen model over the flow parameters can be analyzed. Thus, using dimensionless parameters to discuss the obtained results could filter, hide or change the relevancy of the differences between the results of different constitutive functions. The Reynolds number (Re) was used only as a reference, to make sure the range of the calculations lies in the range of interest. Also, the dimensionless apparent viscosity for high shear rates (η^*_∞) is used to establish the high shear rates viscosity plateau of the theoretical fluid. Their definitions are proposed by Thompson and Soares (2016) and de Souza Mendes *et al.* (2007), respectively:

$$Re = \frac{\rho {V_c}^2}{\tau_0 + K(\frac{V_c}{L_c})^n + \eta_\infty(\frac{V_c}{L_c})} \tag{24}$$

$$\eta^*_\infty = \frac{\eta_\infty \dot\gamma_1}{\tau_0} \tag{25}$$

To compare the results in Section 3, the coefficient of determination (r^2) was used. It provide a measure of how well the models could replicate the reference data, where a r^2 equals to one meant a perfect fit of the data. Although r^2 values usually range from zero to one, it is possible to have negative r^2 values when the fitting function is non linear. A negative r^2 value means that the fitted function has a higher quadratic error than the mean value of the observed values.

$$SSE = \sum_{i=1}^{s} (\phi_i - \hat\phi_i)^2 \tag{26}$$

$$r^2 = 1 - \frac{SSE}{\sum_{i=1}^{s}(\phi_i - \overline{\phi})^2} \tag{27}$$

where s is the number of observations, ϕ_i is the reference value at the observation point i, $\hat\phi_i$ is the value obtained with the proposed model at the observation point i, and $\overline{\phi}$ is the mean value of the reference values. The relative error (e) and the mean error ($\bar e$) are calculated, respectively, by the following expressions:

$$e = \frac{|\hat\phi_i - \phi_i|}{\phi_i} \tag{28}$$

$$\bar e = \frac{1}{s}\sum_{i=1}^{s} e_i \tag{29}$$

2.3 Artificial data

To obtain the rheological data, the SMD$_\infty$ function was employed to generate an artificial flow curve used as raw data for the fitting of different models. The fluid and its parameters were based the data presented by de Souza Mendes and Dutra (2004) for a Carbopol 0.12% wt aqueous solution with $\eta_\infty^* = 0.01$. The parameters used to generate the fluid CS_{SMD_∞} are shown in Tab. 2.

Table 2. Parameters of the SMD$_\infty$ model to generate the artificial data used in Section 3.

Fluid	τ_0 $[Pa]$	K $[Pa.s^n]$	n $[-]$	η_0 $[Pa.s]$	η_∞ $[Pa.s]$
CS_{SMD_∞}	0.354	1.204	0.6508	1782	0.023220

2.4 Solution Method

To solve Eq. (5), a semi-analytic solution was employed as some of the constitutive equations do not allow an analytic solution. A set of a thousand points was used to solve Eq. 5 in terms of $\dot{\gamma}$, for an imposed $\frac{dp}{dx}$, and then a numerical integration was used to obtain the velocity profile. To obtain the flow rate, another numerical integration was realized.

3. RESULTS

In this section, each one of the functions presented in Tab. 1 was used fit the flow curve of the fluid shown in Tab. 2.

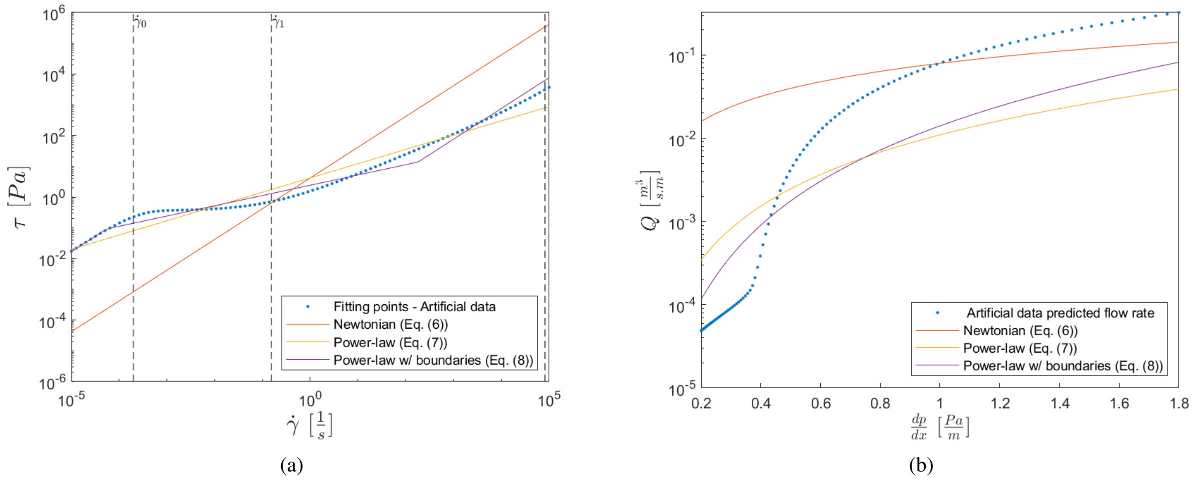

Figure 3. (a) Flow chart and (b) flow rate for the Newtonian model (Eq. (6)), power-law model (Eq. (7)) and power-law model with boundaries (Eq. (8).

As can be seen in Fig. 3, the Newtonian model (Eq. (6)) could not fit the viscoplastic behavior, neither in the flow chart or in terms of flow rate. It is clear that only one parameter is not enough to model such a complex behavior. On the other hand, the power-law model with and without boundaries (Eqs. (8) and Eqs. (7), respectively) showed a relatively good agreement in the flow chart, even with just two parameters in the case of the power-law model. But the agreement in terms of flow rate is very poor, particularly because in the range of Reynolds number considered in this work there is the transition between the low shear rate plateau and the power-law region, and none of this functions predict any transition. As the power-law with boundaries can model three different zones (the low shear rate plateau, the power-law zone, and the high shear rate plateau) it is possible that at a higher (or even lower) range of Reynolds number this model can present a better fit.

Figure 4 presents the flow chart and the flow rate as function of the presure gradient for the Casson (Eq. (12)), Carreau (Eq. (15)) and the Cross (Eq. (16)) models. They show a relatively good agreement at the flow curves, even the Casson model that has only two parameters. But the differences in the flow rate are still substantial. The Carreau and the Cross models share several characteristics, as both model a low shear rate plateau and a high shear rate plateau with apparent viscosity approximately constant, and a power-law region between these zones. Once more, one of the protagonists of the observed behavior of the artificial data is the transition zone, and none of these models have a specific parameter for this region, explaining the difference in the flow rate.

Figure 5 presents the results for the Bingham function and its regularizations. The Bingham function is the simplest function to model the viscoplastic behavior, one of the most used in studies and it has only two parameters, as well as the

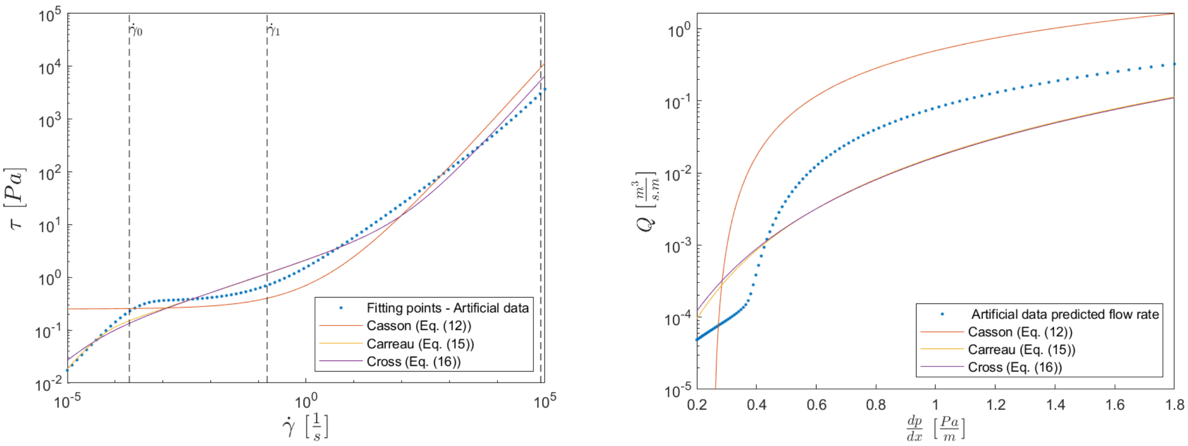

(a) (b)

Figure 4. (a) Flow chart and (b) flow rate for the Casson (Eq. (12)), Carreau (Eq. (15)) and the Cross (Eq. (16)) models.

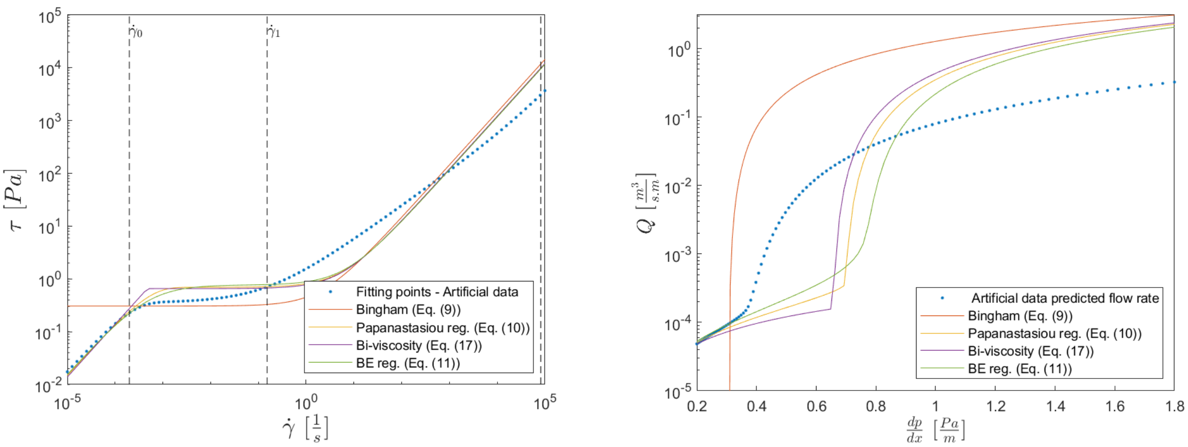

(a) (b)

Figure 5. (a) Flow chart and (b) flow rate for the Bingham function (Eq. (9)) and its regularizations: Papanastasiou model (Eq. (10)), Bercovier and Engelman model (Eq. (11)), and bi-viscosity model (Eq. (17)).

Casson model that can also model the viscoplastic behavior. The Bingham function presents two different regions, one for $\tau < \tau_0$ and other for $\tau \geq \tau_0$, as presented by Eq. (9). In the fist region, $\dot{\gamma} = 0$ and the apparent viscosity is infinite, meaning that this region has similar properties with the low shear rate region already described. The region for $\tau \geq \tau_0$ has a constant apparent viscosity, which is a property of the described high shear rate plateau. Each of the Bingham model regularizations also present these regions, and include a transition region. The bi-viscosity model (Eq. (17)) is the only one that its transition zone does not have its own parameter. The Bercovier and Engelman model (Eq. (11)) and the Papanastasiou model (Eq. (10)) have a regularization parameter that can also be seen as a numeric artifice to ease simulations, although in the present work these parameters were defined in the fitting process. Even presenting the transition region, these models do not model the power-law region, which cause the difference observed in the flow rate (Fig. 5(b)). It is worthwhile to mention that all the regularizations mimic qualitatively well the behavior of the reference function, but they are quantitatively different from each other and the transition start point is also different for each function.

Figure 6 shows the Herschel-Bulkley function (Eq. (13)) and its regularizations. Differently from the Bingham function, the Herschel-Bulkley function has three parameters, and the region for $\tau \geq \tau_0$ is a power-law region. Its regularizations also model the transition region, and the HVP model (Eq. (18)) includes a high shear rate plateau. Therefore, the HVP model has five parameters, while the SMD model (Eq. (19)) and the regularized Herschel-Bulkley model (Eq. (14)) have 4 parameters each, the latter presenting a regularization parameter. With more parameters, it is possible to fit more complex behaviors, but the extra parameter of the HVP model did not allow it to achieve a better fit or a more similar flow rate. The main issue is that with more parameters, it is more difficult to set its values, increasing the errors and the numerical and experimental costs to obtain it. Another important point is that, the more complex the function is, the higher the difficulties of using it in computational fluid mechanics.

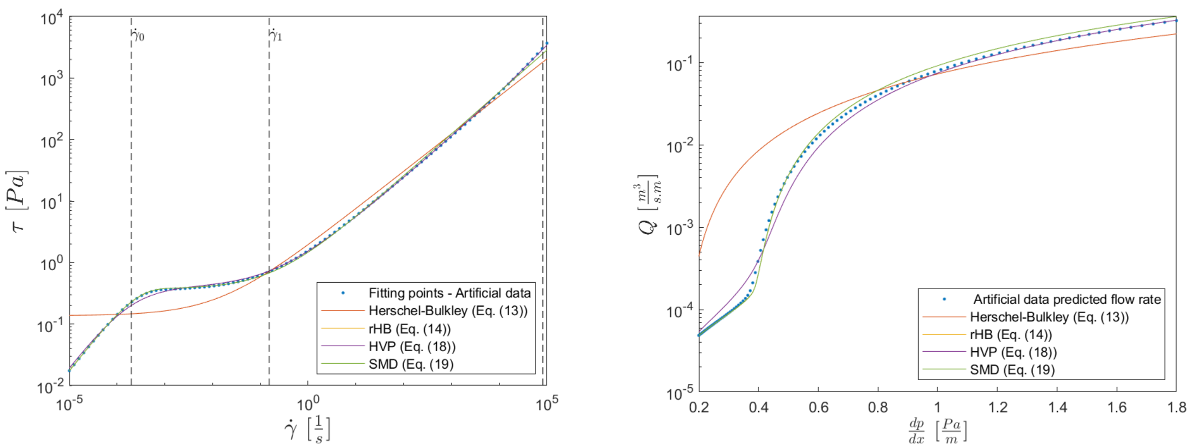

(a) (b)

Figure 6. (a) Flow chart and (b) flow rate for the Herschel-Bulkley function (Eq. (13)) and its regularizations: HVP (Eq. (18)), and SMD (Eq. (19)) models.

Once again, the difference between functions that have a transition zone is made clear: the difference between the Herschel-Bulkley function and its regularizations is clear in both graphs of Fig. 6. But, as each regularization function has a different mathematical artifice to model the transition zone, each function has a different response to the fitting process. At some circumstances, a function can completely fit another, as can be seen comparing Figs. 6(a) and 6(b). Although the agreement in the flow chart is high between the regularizations, the flow rate shows significant differences. This results highlight the importance of the fit in the transition and power-law regions, where smalls detours can lead to significant differences in flow rate. However, the general behavior is qualitatively the same, but can be numerically different.

Table 3 show the coefficient of determination (r^2) for the flow chart fitted curves and the flow rate predicted by each model, in comparison with the artificial data. To better understand the meaning of the r^2_{flow}, the average flow rate error ($\bar{e}$) is shown too. Figure 7 compares graphically the obtained r^2_{fit} and r^2_{flow}. As the flow rate has exponential behavior at this range, the error can varies some orders of magnitude within the range, so Tab. 4 shows some samples of errors for three Re numbers: $Re = 10^{-4}$, 10^0, 10^2, obtained respectively with pressure drops of 0.3867, 0.6773 and 1.9551 $\frac{Pa}{m}$. As each model can have a different Re, these values of Re were calculated with the SMD_∞ function. It is clear that a better r^2_{fit} leads to a better r^2_{flow}, but even with $r^2_{fit} = 0.9988$, the average flow error for the HVP model still as high as 19.34%. This fact shows the importance of the right choice of the model. An error of this magnitude is above any acceptable error induced by the domain discretization when a numerical method is used, for example. Thus, the choice of the model is critical for the simulation. Another point to highlight is that even a small change in the r^2_{fit} can lead to significant errors in the flow rate value. The Cross model, for example, has a $r^2_{fit} = 0.987$ and a $\bar{e} = 130.4\%$, much higher than the SMD equation error.

Table 3. r^2 for the flow chart (r^2_{fit}) and for the flow rate (r^2_{flow}), and the average flow rate error $\bar{e}$.

	r^2_{fit}	r^2_{flow}	$\bar{e}(\%)$
Newtonian (Eq. (6))	-0.316	0.6219	8569
Bingham (Eq. (9))	0.906	-164.1	3573
Casson (Eq. (12))	0.936	-27.33	1103
Power-law (Eq. (7))	0.95	-0.1365	279.4
Bi-viscosity (Eq. (17))	0.96	-53.74	223.9
Papanastasiou reg. (Eq. (10))	0.962	-45.14	191.9
BE reg. (Eq. (11))	0.964	-32.02	150
Herschel-Bulkley (Eq. (13))	0.972	0.8904	991.7
Power-law w/ boundaries (Eq. (8))	0.98	0.103	133.1
Cross (Eq. (16))	0.987	0.2473	130.4
Carreau (Eq. (15))	0.988	0.2623	116
SMD (Eq. (19)	1	0.9739	10.46
rHB (Eq. (14))	1	0.9739	10.29
HVP (Eq. (18))	1	0.9988	19.34

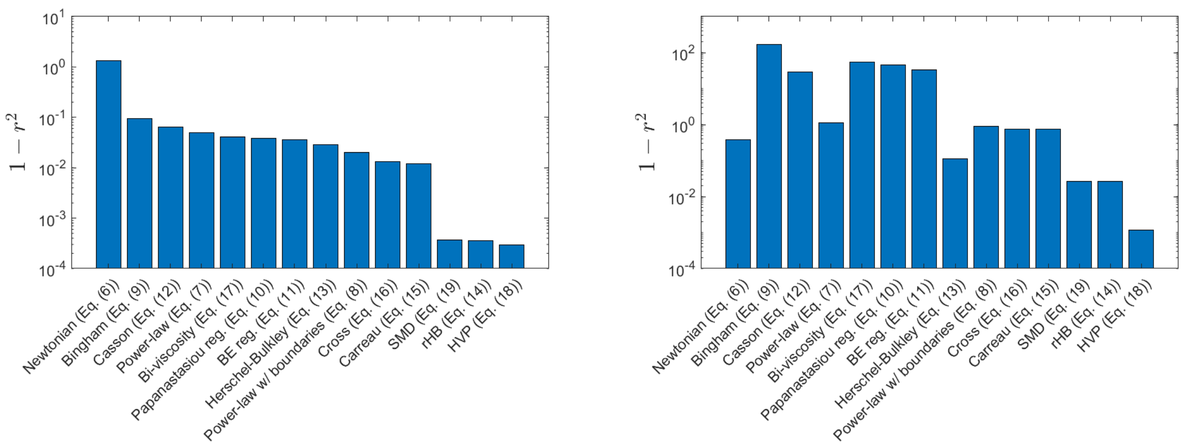

(a) (b)

Figure 7. r^2 for the (a) flow chart (r^2_{fit}) and (b) flow rate (r^2_{flow}).

Table 4. Samples of flow errors at $Re = 10^{-4}$, $Re = 10^0$ and $Re = 10^2$.

	$e_{Re=10^{-4}}(\%)$	$e_{Re=10^{0}}(\%)$	$e_{Re=10^{2}}(\%)$
Newtonian (Eq. (6))	99.16	59.79	143.8
Bingham (Eq. (9))	99.52	96.22	89.0
Casson (Eq. (12))	98.13	87.56	79.66
Power-law (Eq. (7))	81.82	356.3	731.6
Bi-viscosity (Eq. (17))	176.9	557.9	86.32
Papanastasiou reg. (Eq. (10))	128.6	8342	85.75
BE reg. (Eq. (11))	90.66	3843	84.56
Herschel-Bulkley (Eq. (13))	96.66	32.47	47.45
Power-law w/ boundaries (Eq. (8))	68.43	394.5	279.5
Cross (Eq. (16))	67.85	360.8	179
Carreau (Eq. (15))	65.98	355.9	172.5
SMD (Eq. (19)	42.11	11.83	10.64
rHB (Eq. (14))	42.15	11.66	10.64
HVP (Eq. (18))	20.05	23.42	1.80

It is worthwhile to note that a model like the Bercovier and Engelman model, which is essentially a Bingham model regularization, presents a good agreement to the fitting data even not having a power-law zone. This is only possible due to the adopted shear rate fitting range, as a narrower fitting range permits better fittings, and the Bercovier and Engelman model can fit the power-law zone with its transition zone. This would not be possible if the fitting range was wider.

4. CONCLUSIONS

This work discussed the influence of the choice of the constitutive equation in the fully developed flow in a simple channel using a semi-analytic method to solve it. For the majority of fluids, the average variation in flow rate was above 10% when changing from one model to another, even when changing between regularizations of the same model. This value is higher than any acceptable value for the error introduced by the domain discretization when a numerical method is used, for example, showing the importance of the choice of the model. It is worthwhile to mention that the qualitative behavior of all tested models was the same, the only differences are in the numerical values. As expected, functions with a higher number of parameters had a better fitting. The present results indicate that the models used can be swapped without a greater influence over the results.

5. ACKNOWLEDGEMENTS

This study was financed in part by the Coordenação de Aperfeiçoamento de Pessoal de Nível Superior - Brasil (CAPES) Finance Code 001. The author F. Zinani is a grant holder of CNPq-Brazil (Proc. n. 307827/2018-6).

6. REFERENCES

Benmoussa, A., Rahmani, L. and Belkacem, D., 2017. "Simulation of viscoplastic flows in a rotating vessel using a regularized model". *International Journal of Multiphysics*, Vol. 11, pp. 349–358.

Bercovier, M. and Engelman, M., 1980. "A finite-element method for incompressible non-newtonian flows". *Journal of Computational Physics*, Vol. 36, No. 3, pp. 313–326.

Bingham, E.C., 1917. *An investigation of the laws of plastic flow*. 278. US Government Printing Office.

Bird, R.B., Armstrong, R.C. and Hassager, O., 1987. *Dynamics of polymeric liquids. Vol. 1: Fluid mechanics*. John Wiley and Sons, New York.

Burgos, G.R., Alexandrou, A.N. and Entov, V., 1999. "On the determination of yield surfaces in herschel–bulkley fluids". *Journal of Rheology*, Vol. 43, No. 3, pp. 463–483.

Carreau, P.J., 2006. Ph.D. thesis, University of Wisconsin-Madison.

Casson, N., 1959. "Rheology of disperse systems". *Pergamon Press, London*, p. 84.

Cross, M.M., 1965. "Rheology of non-newtonian fluids: a new flow equation for pseudoplastic systems". *Journal of colloid science*, Vol. 20, No. 5, pp. 417–437.

de Souza Mendes, P.R., Naccache, M.F., Varges, P.R. and Marchesini, F.H., 2007. "Flow of viscoplastic liquids through axisymmetric expansions-contractions". *Journal of Non-Newtonian Fluid Mechanics*, Vol. 142, pp. 207–217.

de Souza Mendes, P.R., 2007. "Dimensionless non-Newtonian fluid mechanics". *Journal of Non-Newtonian Fluid Mechanics*, Vol. 147, pp. 109–116.

de Souza Mendes, P.R. and Dutra, E.S.S., 2004. "Viscosity function for yield-stress liquids". *Applied Rheology*, Vol. 14, pp. 296–302.

Ferreira, M.R.d.S., 2018. *Modelagem numérica e mecânica de escoamentos elasto-viscoplásticos tixotrópicos: investigações com uma nova função viscoplástica*. Ph.D. thesis, Programa de Pós Graduação em Engenharia Mecânica da Universidade Federal do Rio Grande do Sul – UFRGS.

O'Donovan, E. and Tanner, R., 1984. "Numerical study of the bingham squeeze film problem". *Journal of Non-Newtonian Fluid Mechanics*, Vol. 15, No. 1, pp. 75–83.

Papanastasiou, T.C., 1987. "Flow of materials with yield". *Journal of Rheology*, Vol. 31, pp. 385–404.

Santos, D.D., Frey, S.L., Naccache, M.F. and de Souza Mendes, P.R., 2011. "Numerical approximations for flow of viscoplastic fluids in a lid-driven cavity". *Journal of Non-Newtonian Fluid Mechanics*, Vol. 166, pp. 667–679.

Thompson, R.L. and Soares, E.J., 2016. "Viscoplastic dimensionless numbers". *Journal of Non-Newtonian Fluid Mechanics*, Vol. 238, pp. 57–64.

7. RESPONSIBILITY NOTICE

The authors are solely responsible for the printed material included in this paper.